A multi-inversion multi-echo spin and gradient echo echo planar imaging sequence with low image distortion for rapid quantitative parameter mapping and synthetic image contrasts

Manhard, Mary Kate; Stockmann, Jason; Liao, Congyu; Park, Daniel; Han, Sohyun; Fair, Merlin; van den Boomen, Maaike; Polimeni, Jon; Bilgic, Berkin; Setsompop, Kawin

Published in:
Magnetic resonance in medicine

DOI:
10.1002/mrm.28761

Received: 24 August 2020 | Revised: 2 February 2021 | Accepted: 12 February 2021

DOI: 10.1002/mrm.28761

FULL PAPER

Magnetic Resonance in Medicine

A multi-inversion multi-echo spin and gradient echo echo planar imaging sequence with low image distortion for rapid quantitative parameter mapping and synthetic image contrasts

Mary Kate Manhard[1,2] | **Jason Stockmann**[1,2] | **Congyu Liao**[1,2] | **Daniel Park**[1] | **Sohyun Han**[1,3] | **Merlin Fair**[1,2] | **Maaike van den Boomen**[2,4] | **Jon Polimeni**[1,2,5] | **Berkin Bilgic**[1,2] | **Kawin Setsompop**[1,2,5]

[1]Athinoula A. Martinos Center for Biomedical Imaging, Massachusetts General Hospital, Charlestown, Massachusetts, USA

[2]Department of Radiology, Harvard Medical School, Boston, Massachusetts, USA

[3]Center for Neuroscience Imaging Research, Institute for Basic Science (IBS), Suwon, Republic of Korea

[4]Department of Radiology, University Medical Center Groningen, University of Groningen, Groningen, Netherlands

[5]Harvard-MIT Division of Health Sciences and Technology, Cambridge, Massachusetts, USA

Correspondence
Mary Kate Manhard, Athinoula A. Martinos Center for Biomedical Imaging, Massachusetts General Hospital, Building 149, Room 2301, 13th Street, Charlestown, MA 02129, USA.
Email: mary.manhard@cchmc.org

Funding information
NIH, Grant/Award Number: F32EB026304, P41EB015896, R01EB019437, R01EB020613, R01MH116173, S10RR019254, S10RR019307, S10RR023043, S10RR023401 and U01EB025162

Purpose: Brain imaging exams typically take 10-20 min and involve multiple sequential acquisitions. A low-distortion whole-brain echo planar imaging (EPI)-based approach was developed to efficiently encode multiple contrasts in one acquisition, allowing for calculation of quantitative parameter maps and synthetic contrast-weighted images.

Methods: Inversion prepared spin- and gradient-echo EPI was developed with slice-order shuffling across measurements for efficient acquisition with T_1, T_2, and T_2^* weighting. A dictionary-matching approach was used to fit the images to quantitative parameter maps, which in turn were used to create synthetic weighted images with typical clinical contrasts. Dynamic slice-optimized multi-coil shimming with a B_0 shim array was used to reduce B_0 inhomogeneity and, therefore, image distortion by >50%. Multi-shot EPI was also implemented to minimize distortion and blurring while enabling high in-plane resolution. A low-rank reconstruction approach was used to mitigate errors from shot-to-shot phase variation.

Results: The slice-optimized shimming approach was combined with in-plane parallel-imaging acceleration of 4× to enable single-shot EPI with more than eight-fold distortion reduction. The proposed sequence efficiently obtained 40 contrasts across the whole-brain in just over 1 min at 1.2 × 1.2 × 3 mm resolution. The multi-shot variant of the sequence achieved higher in-plane resolution of 1 × 1 × 4 mm with good image quality in 4 min. Derived quantitative maps showed comparable values to conventional mapping methods.

Conclusion: The approach allows fast whole-brain imaging with quantitative parameter maps and synthetic weighted contrasts. The slice-optimized multi-coil shimming

and multi-shot reconstruction approaches result in minimal EPI distortion, giving the sequence the potential to be used in rapid screening applications.

KEYWORDS
low distortion EPI, multi-shot acquisitions, quantitative mapping, synthetic imaging

1 | INTRODUCTION

Echo planar imaging (EPI) is a well-established approach for rapid acquisition schemes in MRI. However, EPI is not typically used for structural imaging, as it is sensitive to B_0 inhomogeneities that cause undesirable image distortion and T_2^* decay that causes blurring, both along the phase encoding direction. The EPI-related distortion and blurring can be reduced using parallel imaging with high acceleration factors, although often at the cost of signal-to-noise ratio (SNR) and image quality.

Recent advances in reconstruction approaches and hardware technology have shown potential in overcoming the geometric distortion in EPI. Combined radiofrequency (RF) and B_0 shim array hardware[1-3] has demonstrated the ability to significantly reduce B_0 inhomogeneity and hence distortion from EPI by dynamically shimming each slice, while retaining the high receive sensitivity needed from a brain receive array for EPI acquisitions. Additionally, multi-shot EPI acquisitions allow for high in-plane acceleration factors per EPI-shot in order to limit the EPI distortion and blurring, while also shortening the echo-train length of high-resolution imaging to allow shorter-TE acquisitions with higher signal. While multi-shot EPI is prone to image artifacts from shot-to-shot phase variations, low-rank reconstruction approaches[4-6] have enabled multi-shot EPI with high in-plane acceleration factors to be reconstructed robustly without use of additional navigators by enforcing a Hankel structured low-rank constraint in k-space on the phase variation between shots.

Here, we implemented both of these emerging approaches for reducing EPI distortion to enable fast but high-quality imaging with EPI. To take advantage of the improved EPI-encoding capability afforded by these approaches, an efficient EPI-based sequence was developed to rapidly acquire a large number of multi-inversion, multi-echo images.[7] The resulting multi-contrast images were then able to be used to compute quantitative parameter maps with high spatial fidelity, including T_1, T_2, and T_2^* maps, from a single scan.

Furthermore, synthetic weighted images of clinical contrasts, including T_1 weighted, T_2 weighted, T_2^* weighted, and T_2 FLAIR, can be generated from the quantitative parameter maps found from the proposed EPI-based sequence. In typical clinical MRI acquisitions, images are weighted by sequence parameters and are somewhat long, on the order of several minutes per contrast-weighted acquisition. These acquisitions are also typically acquired sequentially to obtain the desired set of different contrasts. In addition, contrasts can vary across acquisitions due to B_1 inhomogeneity, coil sensitivities, or RF pulse settings. This variation in signal intensity results in images that can only be compared relatively across time. While quantitative MRI is not routinely used in clinical settings, it has many advantages in robustness and repeatability that may benefit diagnoses and interpretation. The synthetic image approach allows for images to be created quickly in post-processing rather than individually acquiring each desired contrast. Recently, other emerging EPI-based techniques[8-10] have also explored the acquisition of many clinical contrasts in one fast scan. Here, we look to limit the distortion of images that use this type of approach, while still keeping the scan time low. Our proposed approach rapidly acquires quantitative maps and synthetic images with full brain coverage and no slice gaps, between 1 and 4 min in total for the protocols demonstrated here.

2 | METHODS

2.1 | Acquisition and sequence design

Figure 1 shows the pulse sequence diagram that was used in the study. In short, a previously established multiple inversion, multiple slice acquisition[11-13] was performed, which plays a non-selective adiabatic inversion pulse followed by the acquisition of all slices, resulting in a different inversion time (TI) for each slice. The acquisition is repeated eight times with a shifted slice ordering, so that over the repetitions, each slice sees a range of TIs adequate for fitting T_1 maps. In this work, during each slice acquisition, a multiple spin-and-gradient echo (SAGE)[14,15] approach is incorporated into the sequence to allow for both gradient echo (GRE) single-shot EPI readouts as well as asymmetric spin echo single-shot EPI readouts. Here, two GRE EPI readouts are used followed by three asymmetric spin echo EPI readouts, so that both T_2 and T_2^* maps can be fit for each slice. To further improve the acquisition efficiency of the proposed sequence, simultaneous multi-slice (SMS) acquisition[16-18] with multiband (MB) RF pulses and blipped-CAIPI[19] was also incorporated. An in-house B_0 shim array coil was used to mitigate EPI-based distortion effects (see section *B_0 Shim Array*).

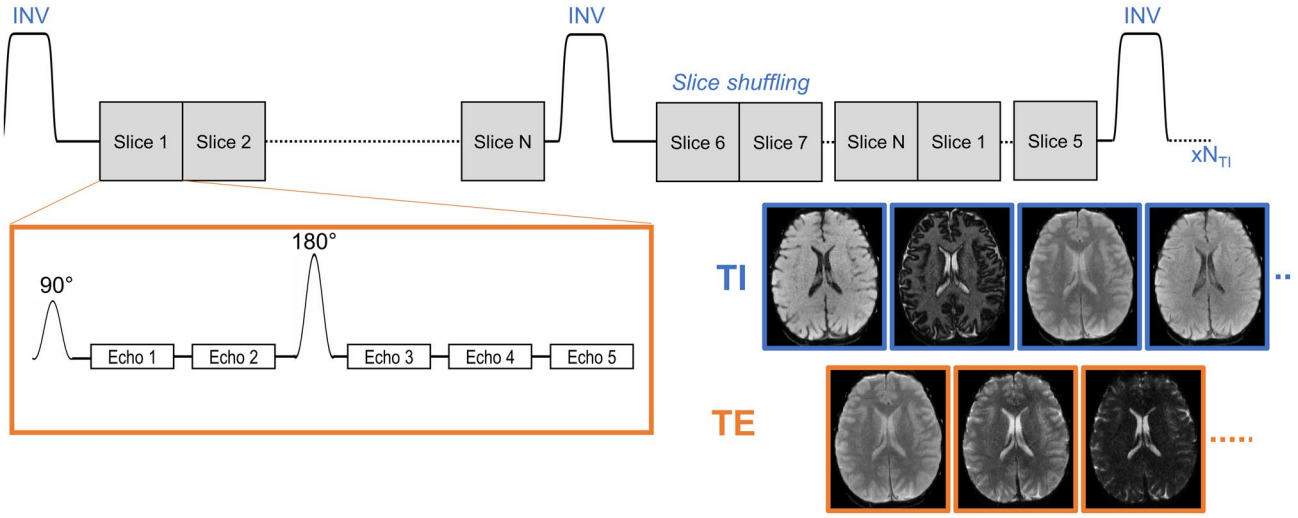

FIGURE 1 Pulse sequence for multi-inversion, multi-echo EPI acquisition. A nonselective inversion pulse is used, followed by the acquisition of all slices. This is repeated up to N_{TI} repetitions, with a shuffled slice order for each repetition. Therefore, each slice sees a range of different TIs, as shown in example images in the blue boxes. In addition, each slice acquisition consists of multiple spin and GREs, as shown in the orange box, resulting in images with different TEs, shown in the images with orange boxes on the right

To mitigate large distortion and blurring, without requiring specialized hardware as well as achieving high resolution imaging with shorter TEs, a multi-shot interleaved-EPI version of the proposed sequence was also developed. Here, the EPI-interleaves for each shifted slice ordering were acquired in sequential TRs to minimize time gaps between these shots, so that potential artifacts from both bulk motion and phase variation could be reduced. To reduce spin history effects that can create signal variations across the EPI interleaves, a dummy TR is inserted prior to the acquisition of each shifted slice ordering, at the cost of a 33% increase in scan time.

2.2 | B_0 shim array

Single shot images were acquired with an in-house 32-channel brain receive array that uses inductive chokes to incorporate DC current-carrying capability into each receive loop to use for local B_0 shimming (using an "AC/DC" or "iPRES" design approach).[1,3] After the second-order global shims were applied using the vendor-provided shim adjust tool, the AC/DC coil was used to apply high-spatial order B_0 offsets to mitigate the remaining B_0 inhomogeneity (ΔB_0) in the brain on a slice-by-slice basis. The low inductance and minimal eddy currents of the shim array coils allows shim currents to be rapidly switched in between repetition times (TRs) without introducing image artifacts. A basis set of calibration B_0 maps were first derived from a two-echo GRE acquisition. A constrained optimization routine[3] was then used to solve for shim currents in each channel subject to a least squares penalty on the residual ΔB_0 in the slice of interest after the shim field has been applied. For SMS acquisitions, a slice-group by slice-group shimming was also adapted to obtain good shimming performance across the simultaneously acquired slices as previously demonstrated in Liao et al.[20] When in-plane and/or SMS acceleration were used, the dynamic shims were also updated during acquisition of the autocalibration k-space lines in order to ensure consistency with the image volume k-space lines.

For expedience during scanning experiments, the vendor-provided online shim adjust tool was used to perform second-order B_0 shimming at the beginning of each scan. To demonstrate the benefits of this multi-coil (MC) slice-optimized shimming, B_0 maps were acquired using a two-echo GRE acquisition using the standard second-order global shim and compared to the predicted slice-optimized shim. Figure 2A shows baseline and predicted B_0 maps in several representative slices for three subjects with the SD of ΔB_0 across slices shown at the bottom in blue. The inhomogeneity (and, therefore, the voxel shift in the EPI acquisitions) is noticeably improved using the dynamic slice-optimized MC shimming approach, with the percent improvement shown across slices. The SD of ΔB_0 across the whole brain was on average 29 Hz across subjects with the standard global shim, which improved to an average of 16 Hz using the slice-optimized MC shimming approach. In addition, for one subject, single shot EPI sequences with no acceleration were acquired in both the anterior-posterior (AP) and posterior-anterior (PA) directions, to enable a comparison of EPI distortion that is present due to B_0 inhomogeneity. This was repeated with both the standard second-order global shim and the dynamic shimming approach. Figure 2B shows these single shot EPI images in one slice, where severe and opposing distortions causing voxel pileup and stretching can be seen using the global second-order shim. In this particular slice,

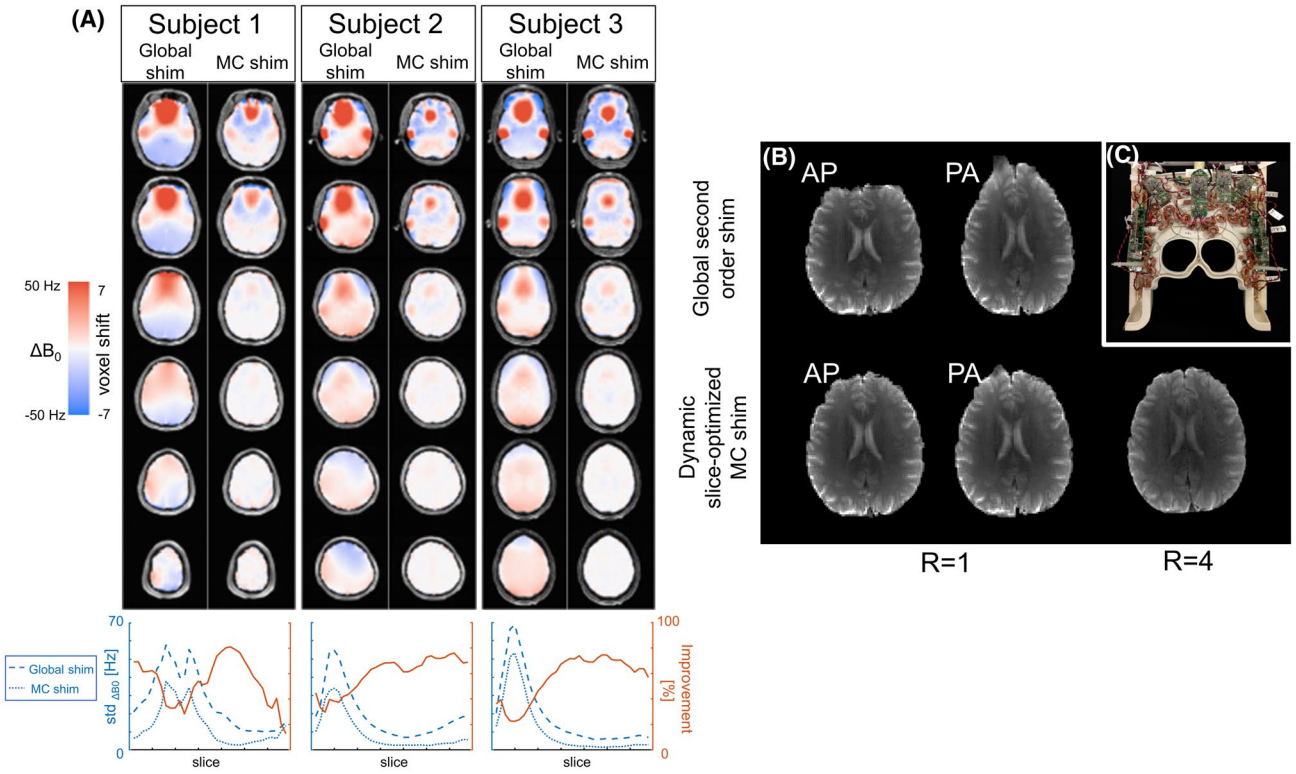

FIGURE 2 Demonstration of EPI distortion improvements using a dynamic shim coil. A, B0 maps overlaid on anatomical images from three subjects in several slices, comparing a global second order shim and a predicted dynamic slice-optimized MC shim. The B_0 maps also show the corresponding voxel shift that would occur with a single shot acquisition with no acceleration (1.2 mm acquisition with echo spacing = 0.76, number of phase encode lines = 188). The B_0 inhomogeneity and voxel shift is visibly improved using the dynamic shim approach. Below, the SD of B_0 is shown across slices from foot to head for both the global shim and MC shim approaches in the three subjects in blue, with the percent improvement shown in red. B, The improvement in image distortion is demonstrated in one slice, where a single shot EPI acquisition with no acceleration acquired in both the AP and PA directions shows severe distortion when using a global shim (top), compared to a much-improved distortion using a dynamic slice-optimized MC shim (bottom). The distortion with R = 4 and the dynamic MC shimming is very low. C, The 32-channel AC/DC coil is pictured

distortion is reduced when using the dynamic shim by 75%, and again decreased by four-fold when using an acceleration factor of 4.

Across subjects, the improvement in B_0 homogeneity from the dynamic MC shimming approach results in a reduction in EPI distortion by 52% without SMS and 45% for an SMS acquisition with a MB factor of 2. Overall, we can expect approximately 50% improvement in distortion; for example, an EPI image with an acceleration factor of R = 4 leads to a distortion level closer to what is typically seen with an R = 8 acquisition. For a retrospective comparison of second-order and MC shim performance, the B_0 field maps were processed offline using a second-order shim basis with the same brain mask and shim optimization solver used for the MC shimming experiments. This provided a modest 16% improvement in the SD of B_0. Comparing the MC shim to this offline, optimal second-order shim, the gains provided by the MC hardware are reduced to 44% and 36% for SMS1 and SMS2, respectively.

2.3 | In vivo study

The sequence was acquired on a Siemens 3T Prisma scanner in nine healthy volunteers in total, with Institutional Review Board approval and written informed consent. The AC/DC coil was used in four of the subjects, while a 32- or 64- channel vendor provided coil was used in the other five subjects. Several protocols were demonstrated, described here as protocols A, B, and C. Protocols A and B both utilize the dynamic slice-optimized MC shimming approach combined with a single-shot acquisition. For these protocols, a B_0 map was found from a dual-echo GRE acquisition at 2 mm isotropic resolution with TEs = 4.6/7.0 ms and TR of 400 ms (90 s scan time). To further improve resolution and develop a distortion limited protocol in cases where an AC/DC coil may not be available, a multi-shot approach is shown in protocol C.

For protocol A, a single shot acquisition using the 32-channel AC/DC coil (for both RF signal reception and B_0

shimming) with in-plane acceleration factor R = 4 was implemented with 1.2 × 1.2 mm resolution (field of view [FOV] = 220 × 220 mm), a partial Fourier factor of 6/8, and five echo times (TEs; two gradient and three mixed spin echoes) with TEs = [14 43 96 125 153] ms, and a TR = 7.8 s with eight TIs (first TI = 25 ms) with shifted slice orderings. This required a total scan time of 63 s, plus an additional 31 s to acquire an EPI-based reference scan for parallel imaging. The acquisition produced 40 slices, with a slice thickness of 3 mm, shifting the slice ordering by five slices every TR.

Protocol B was similar to protocol A, using the AC/DC coil with R = 4 in-plane acceleration, but in addition used an SMS acquisition with MB = 2 for a total acceleration factor of 8. This acquisition also used similar sequence parameters but a reduced TR = 4 s, for a total scan time of 32 s plus an additional 40 s for the EPI-reference scan, where separate reference data are acquired for SMS calibration and in-plane calibration. The acquisition used a slice thickness of 3 mm for 40 slices and shifted the slice ordering by 3 slice groups to distribute the TIs over the eight repetitions for all 20 slice groups. Other sequence parameters include TEs = [14 43 96 125 153] ms, a first TI = 25 ms, and a resolution of 1.2 × 1.2 mm with FOV = 220 × 220 mm.

Protocol C was acquired with a standard vendor provided 32- or 64-channel head coil, using an in-plane acceleration factor of R = 8 and three EPI interleaves, plus an additional dummy shot to reduce spin history signal differences between shots as described above. This results in the use of four measurements *per* shifted slice ordering. The higher acceleration factor also allowed for higher in-plane resolution of 1 × 1 mm at reasonable TEs, with a slice thickness of 4 mm. More sequence parameters include TEs = [18 45 83 110 138] ms, TR = 7 s, first TI = 25 ms, with eight shifted slice orderings, FOV = 220 × 220 mm and 40 slices, and no partial Fourier factor for a total scan time of 3 min 58 s, not including reference scan time.

Since the EPI-reference scan used for parallel imaging reconstruction can take up a significant portion of the overall scan time in the above protocols, we investigated the potential in replacing these EPI-reference scans with a rapid GRE-based reference scan. The EPI-based reference scan takes longer to acquire because each interleave is collected separately, but it ensures that any distortion that occurs in the image from the EPI acquisition is matched in the calibration data. However, in the above protocols where the distortion from EPI is minimized, a distortion-free GRE-based reference scan may suffice and allow for very short calibration scan times. This was tested and verified in one subject for the acquisition with parameters for protocol C, where images reconstructed from both EPI and GRE calibration scans gave very similar results, which is shown in Supporting Information Figure S1, which is available online. In this case, the calibration scan time for 96 k_y lines with an EPI-based reference scan was 56 s across 40 slices, and with a 2D GRE-based reference scan across the same number of k_y lines and slices, with a TR = 5.5 ms was 21 s. Using the ESPRIT algorithm,[21] it was determined that 16 k_y lines were sufficient to provide robust coil sensitivity maps which were used to reconstruct data in Figure S1, which would result in a GRE calibration scan time of 4.4 s, including four dummy TRs per slice. As such, a GRE reference scan with 16 k_y lines was employed for all reconstruction of protocol C data.

For one subject, quantitative maps from the proposed EPI-based acquisition in protocol C were compared to maps obtained using conventional mapping methods. To derive quantitative T_2^* maps, a multi-echo GRE sequence with TE = [4 10 16 22 28 34] ms, TR = 389 ms, resolution = 1 × 1 × 4 mm and FOV = 256 × 256 mm was acquired in a scan time of 2 min 54 s. To quantify T_2 values, four single slice single spin echo acquisitions with TEs = [12 24 36 48] ms, TR = 2 s, with a resolution = 1 × 1 × 4 mm and FOV = 256 × 256 mm were acquired in a total scan time of 18 min and 48 s. An inversion recovery sequence was used to quantify T_1 values, modestly accelerated to achieve a reasonable scan time, using a TSE factor of 4 and R = 2 in-plane acceleration. Eight TIs were acquired separately, TI = [25 100 200 400 800 1600 2400 3200] ms, with 256 × 256 mm FOV, and 1 × 1 × 4 mm resolution, with TE = 17 ms and TR = 7.8 s, for a total scan time of 37 min.

To further investigate consistency and repeatability of the proposed approach, two additional measurements were made. First, the three proposed protocols were compared in one subject with the standard 32-ch head coil, no dynamic shimming, and a matched slice resolution of 4 mm to minimize changes in through-slice dephasing. Quantitative maps were compared across the three protocols after downsampling all to the same in-plane resolution (1.2 mm) and partial Fourier factor (6/8). Second, protocol A was acquired three times in one subject (no repositioning), to quantitatively compare the resulting maps from the three repeated scans.

The derived synthetic images were also compared to typically acquired contrasts in the brain in one subject, with matching resolution and coverage. Sequence parameters include: T_1-weighted with TE/TR/TI = 2.41/1500/1200 ms in 3 min 21 s, T_2^*-weighted with TE/TR = 30/38 ms and flip angle = 15° in 3 min 27 s, a T_2-weighted image with TE/TR = 75/7000 in 1 min 40 s, and T_2-FLAIR with TE/TR/TI = 71/8000/2050 ms in 3 min 14 s.

2.4 | Image reconstruction

Single-shot EPI acquisitions (protocols A and B) were reconstructed online using standard scanner software. Multi-shot EPI acquisitions (protocol C) were reconstructed offline using in-house MATLAB scripts. Coil sensitivities were estimated

using an ESPIRIT approach[22] and used in a SENSE-based parallel imaging reconstruction. A multi-shot EPI with low-rank matrix completion reconstruction (MUSSELS[6]) approach was used to minimize potential reconstruction artifacts from shot-to-shot phase variation by jointly reconstructing multiple shots and enforcing a Hankel structured low-rank constraint on the phase variation between shots, where the reconstruction time was approximately 100-200 s per image. A low resolution, Hamming filtered background phase estimate was then found for each shot and removed before taking the mean image across shots to avoid bias that results from averaging magnitude data.[23] This combined real-valued image was used in further processing for quantitative mapping and evaluation.

2.5 | Parameter mapping and synthetic image generation

All images contrasts across TE and TI were fit together using a dictionary matching approach to the signal evolution based on Bloch simulations, on a voxel-by-voxel basis. The dictionary was simulated with instantaneous RF pulses and included the dummy repetitions used to reach steady state. The dictionary included a range that would be expected in brain tissue, with T_2 values and T_2^* values [10:1:100,102:2:200,204:4:400,420:20:600] ms, and T_1 values [400:100:800,810:10:1100,1200:100:2000,2400:400:4800] ms. In addition, the dictionary included an estimate of correction term δ, with δ values [0.5:0.1:1.8], where δ relates the signal before and after the refocusing pulse to account for differences in slice profile and B_1^+ inhomogeneity.[14,24] This gave a total dictionary size of ~11,675 k (1.6 GB), excluding unreasonable values such as $T_2^* > T_2$, which took about 98 min to calculate in our MATLAB implementation. To improve noise in the estimated maps and since the B1 inhomogeneity varies smoothly across space, the δ parameter was then fit to a 2D polynomial to enforce a smooth profile, and maps were re-estimated with a fixed δ in the dictionary fit. This resulted in ~834k dictionary points (133 MB), which were calculated in around 7 min. The dictionary only needed to be calculated once per protocol, and then could be applied to all subject acquisitions. The dictionary matching step is completed in less than 5 min per slice. Relative proton density (PD) maps were found from the normalized difference between the dictionary fit and the data signal evolution.

The quantitative maps were then used to create synthetic images using typical sequence parameters and conventional analytical models to show images of standard clinical weighting. The synthetic images could be created quickly (<1 s) from the previously derived quantitative maps. T_1-weighted (T_1w) images were created with an TI of 1.2 s and a TR of 1.5 s. The T_2-weighted (T_2w) image had a spin echo TE of 75 ms, and a TR of 7 s. The T_2^*-weighted (T_2^*w) images had a TE of 30 ms, a TR of 38 ms, and a flip angle of 15°. T_2-FLAIR images were created with an TI of 2.05 s, a TR of 8 s, and a TE of 70 ms.

2.6 | Validation and analysis

To further validate the quantitative maps, the results from the multi-shot protocol C acquisition were compared to conventional mapping approaches. Conventional T_2^* and T_2 maps were calculated by performing a voxel-wise mono-exponential fit of the echo images to the signal equation. The inversion recovery images were used to fit T_1 maps using a robust model[25] that is insensitive to parameters such as TR or flip angle. Quantitative maps acquired with conventional methods were compared to the quantitative maps from the multi-contrast EPI sequence from the same slice. Several regions of interest (ROIs) were defined as 7 × 7 voxel boxes throughout the slice, and a Bland-Altman analysis was performed on the ROIs of each T_1, T_2, and T_2^* image to evaluate the agreement between maps.

This same ROI-based approach was used to investigate the agreement between protocols, as well as the repeatability of one protocol in the same subject. To evaluate the agreement between protocols, we performed Tukey's tests between protocols. We also report the normalized root mean square error (RMSE) between the dictionary data and each voxel fit across the ROIs for each protocol. For the repeatability analysis, we report the mean and SD across ROIs from different acquisitions, as well as the coefficient of variation across the repeated acquisitions. All statistical analyses were performed using statistical software (GraphPad Prism, version 9).

3 | RESULTS

Figure 3A from the single-shot acquisition with the 32-channel AC/DC coil (protocol A) shows quantitative T_1, T_2, T_2^* and relative PD maps from three representative slices in one subject, acquired in 1.5 min. Figure 3B shows synthetic weighted images from the middle slice, including T_1w, T_2w, T_2^*w, and T_2-FLAIR contrasts generated from the quantitative maps in that slice. The contrasts of these images are similar to those that would be expected from an image acquired with these weighted parameters, although the turbo spin echo (TSE) sequence that is typically used in T_2w and T_2-FLAIR image acquisitions causes additional magnetization transfer (MT) weighting[26] that is not present in the synthetic images here. The technique was also shown to be amenable to SMS acquisitions, as demonstrated in Figure 4 (protocol B). Quantitative T_1, T_2, T_2^*, and relative PD maps are shown in two slices, with the resulting synthetic images

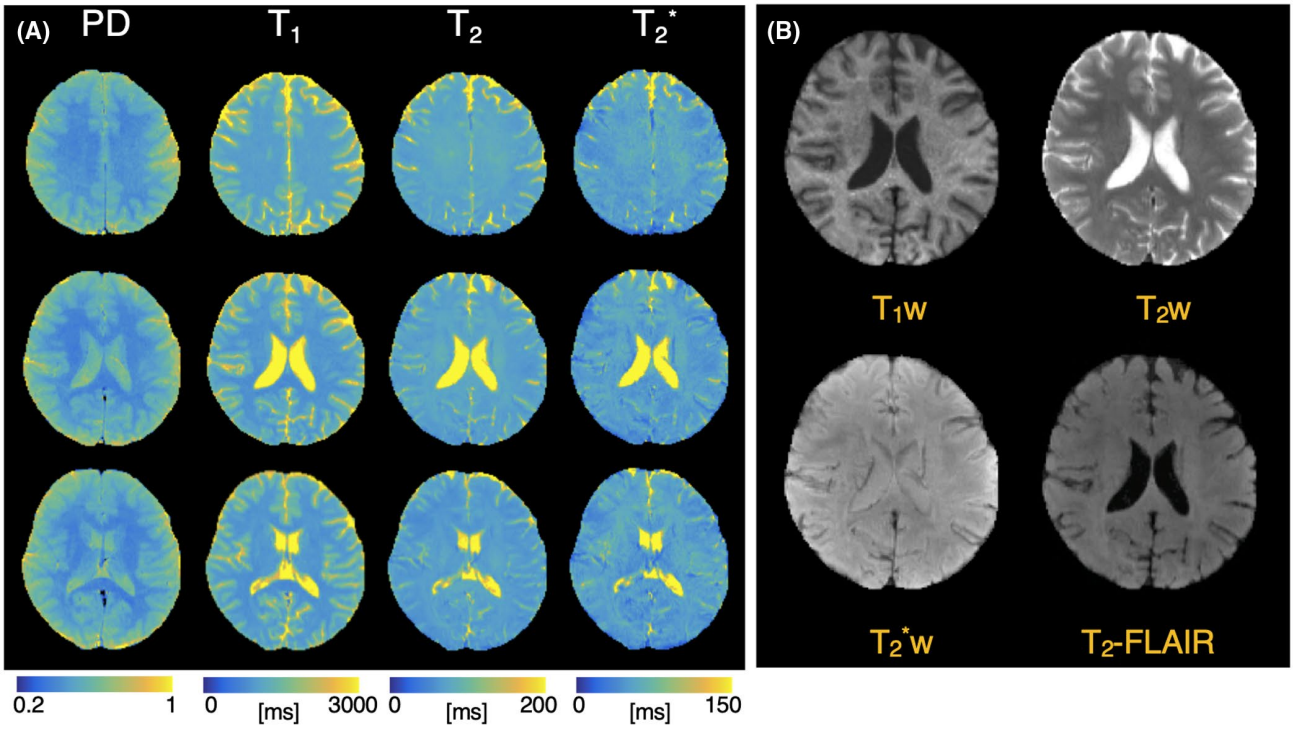

FIGURE 3 A, Quantitative parameter maps from protocol A, single-shot R = 4, acquired with dynamic slice-optimized MC shimming, in three representative slices. B, Synthetic weighted contrasts derived from the middle slice in A, with T_1w, T_2w, T_2^*w, and T_2-FLAIR images

generated in these slices. This SMS protocol allowed for a very efficient scan and could generate whole brain images in a scan time of just over a minute, including the EPI reference scan.

Quantitative maps and synthetic contrasts generated from multi-shot images (protocol C) acquired with a GRE calibration scan are shown for two representative slices in Figure 5. The multi-shot approach produces good quality maps and images at a higher in-plane resolution of 1 × 1 mm acquired in 4 min, and the low-rank reconstruction results in no apparent artifacts from shot-to-shot phase variation. These images also have limited distortion due to the high in-plane acceleration factor, despite being acquired with conventional shimming techniques and a standard head coil.

The quantitative maps from protocol C were validated against conventional mapping techniques, and resulting maps are displayed in Figure 6. Overall, good agreement is seen between the quantitative maps acquired with both the multi-contrast EPI method and the conventional mapping methods. Five ROIs are shown on the slice, and the results from the Bland-Altman analysis are shown in Figure 7. The ROIs show similar values between methods and all points were within the limits of agreement, although some slight biases (T_1: −41 ms, T_2: −5 ms, T_2^*: 3 ms) remain.

The quantitative maps derived from the three presented protocols A, B, and C also display similar results as shown in one slice in Figure 8. Five ROIs from this slice were also analyzed and resulting mean values are shown in Figure 9 with error bars showing the SD in the ROIs. Protocols A and C show very similar T_1 maps (no statistically significant differences), although T_1 values are slightly elevated in protocol B (mean increase of 120 ± 20 ms, $P < .01$, 98 ± 16 ms, $P < .01$ from protocols A and C, respectively). Protocols A and B show very similar T_2 values (no statistically significant difference), while protocol C shows slightly higher T_2 values (mean increase of 6 ± 1 ms, $P < .01$, 7 ± 1 ms, $P < .05$ from protocols A and B, respectively). There were no statistically significant differences between T_2^* values for any protocol. The normalized RMSE between the data and the dictionary across the 5 ROIs were 8.1 ± 1.0%, 9.3 ± 0.9%, and 6.4 ± 0.7% for protocols A, B, and C, respectively. Additionally, the repeated measurements in one subject of Protocol A gave consistent quantitative maps, as shown in Supporting Information Figures S2 and S3. The mean coefficient of variation across ROIs for these repeated measurements were 0.44%, 1.31%, and 2.79% for T_1, T_2, and T_2^*, respectively.

The synthetic images were also compared to clinical contrast-weighted scans as shown in Figure 10. There is similar contrast for all four image types across gray matter, white matter, and cerebrospinal fluid (CSF), although the TSE-based images (T_2-FLAIR and T_2-weighted) have the expected MT weighting that is not present in the synthetic images. In the T_2-FLAIR synthetic image, a white rim in the boundary between gray matter and CSF can be seen particularly in the slice on the bottom left which is not present in

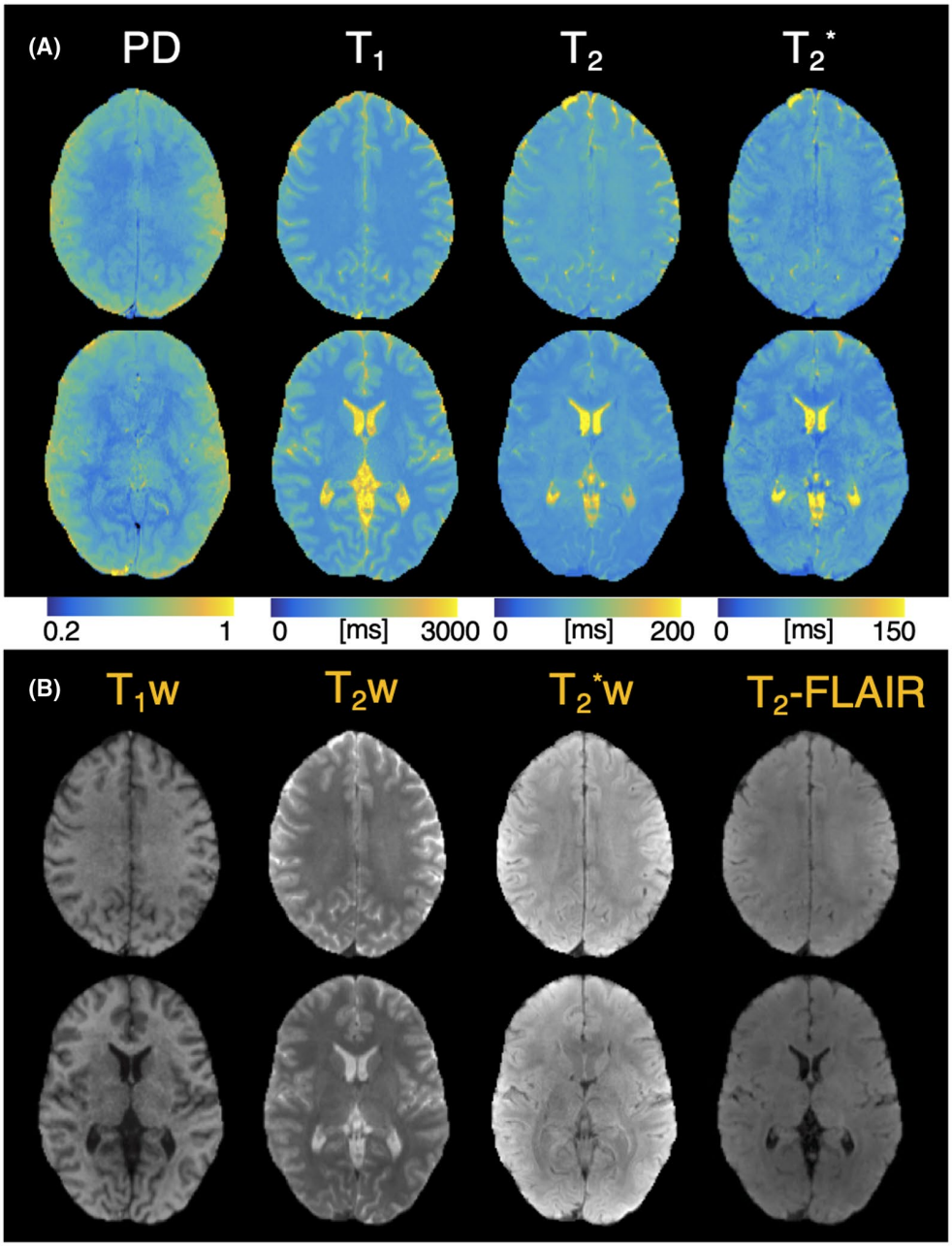

FIGURE 4 A, Quantitative parameter maps from two slices from protocol B, an MB acquisition (MB = 2, in-plane R = 4). B, Synthetic weighted contrasts from both slices show T_1w, T_2w, T_2^*w, and T_2-FLAIR images

the conventional image. Furthermore, the bottom slice shows through-slice intravoxel dephasing in all contrasts from the EPI-based acquisition, as can also be observed in the standard T_2^* image.

4 | DISCUSSION

The presented sequence allows for fast, whole brain images with quantitative parameter maps and a range of synthetic weighted images of standard clinical contrasts, acquired in 1-4 min. While the images are acquired with EPI, the AC/DC coil with slice-optimized MC shimming and multi-shot reconstruction approaches allow for distortion artifacts to be minimized. While synthetic images provide a more immediate clinically applicable screening protocol, as they improve support for clinicians who are trained to perform clinical diagnoses on images with specific weightings, quantitative mapping approaches have many benefits when they can be accurately and quickly acquired, as they allow for consistent and robust results.

The approach presented has similarities to other rapid EPI-based approaches for a fast, full brain exam, such as EPIMix.[10] Our approach has the added benefits of low

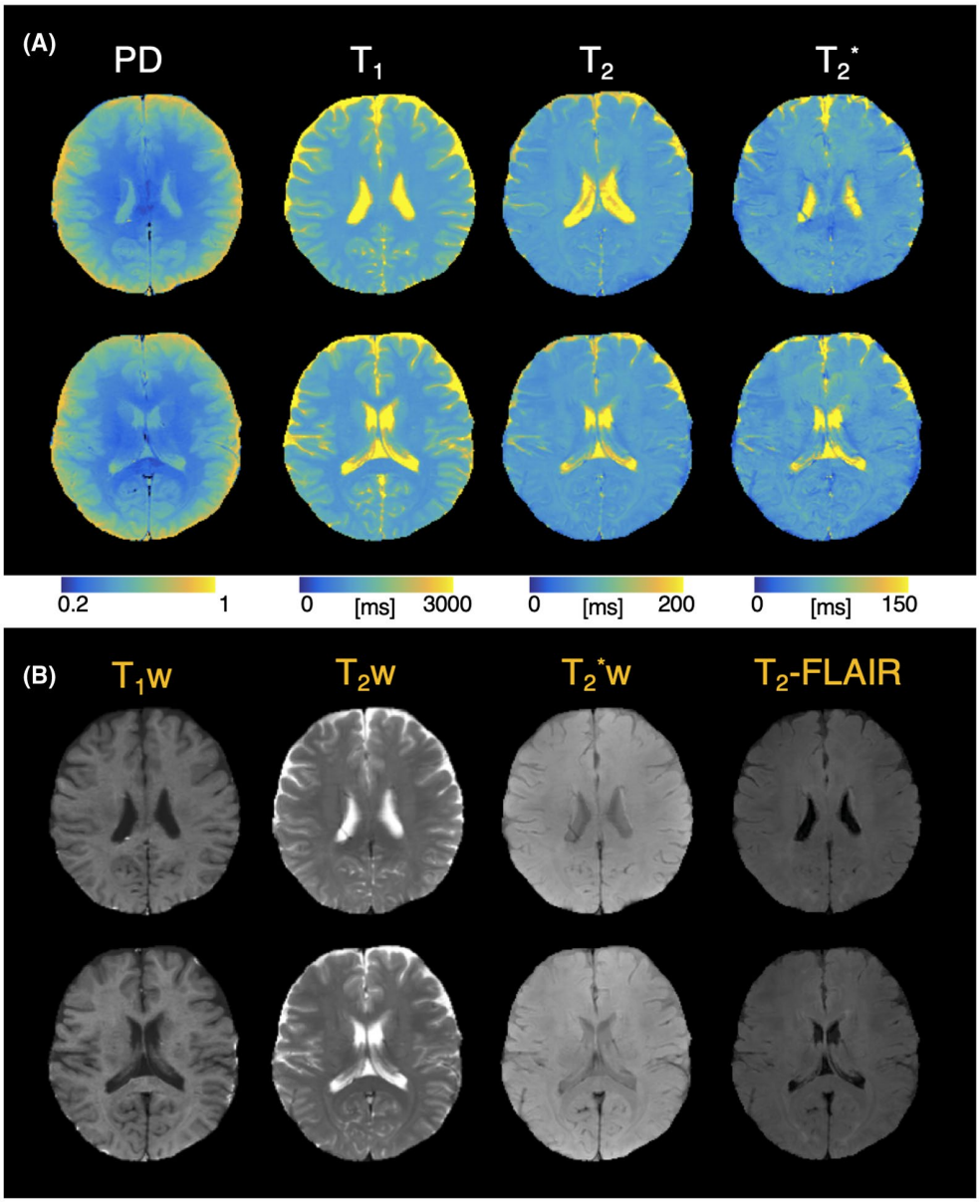

FIGURE 5 A, Quantitative parameter maps from two slices from protocol C, a multi-shot acquisition (R = 8, 3 shots). B, Synthetic weighted contrasts derived from parameter maps of both slices, showing T_1w, T_2w, T_2^*w, and T_2-FLAIR images

distortion and simultaneous acquisition of quantitative parameter maps. However, unlike the EPIMix approach, our current implementation does not have any diffusion weighting, which is often needed in a typical brain MRI exam. Future developments will look to incorporate diffusion weighting into the acquisition to achieve a more complete brain MRI exam. Other imaging approaches using multiple-dynamic multi-echo acquisitions[27,28] have also shown great promise for synthetic imaging derived from quantitative T_1, T_2, and PD parameter maps, albeit at a slightly longer scan time (~5 min) than the approach presented here.

The simultaneous quantitative maps resulting from this multi-contrast EPI approach showed good agreement with conventional mapping techniques, and time constants were within ranges shown in the literature[29,30] at 3T. The T_1 maps from the multi-contrast approach showed slightly higher values in some ROIs compared with the conventional inversion recovery method. This could be due to different RF pulses, since the proposed multi-contrast sequence uses an adiabatic inversion pulse, whereas the conventional approach in this work uses a standard inversion pulse, which is more sensitive to B_1 inhomogeneity. Alternatively, the amount of MT contrast may be different due to the number of refocusing pulses per TR in the multi-contrast approach, leading to differences in the T_1 maps. T_1 maps from the multi-contrast approach may also have differences due to MT between slices, as the slice ordering causes some slices to experience more MT than others. The T_2 maps from the multi-contrast approach

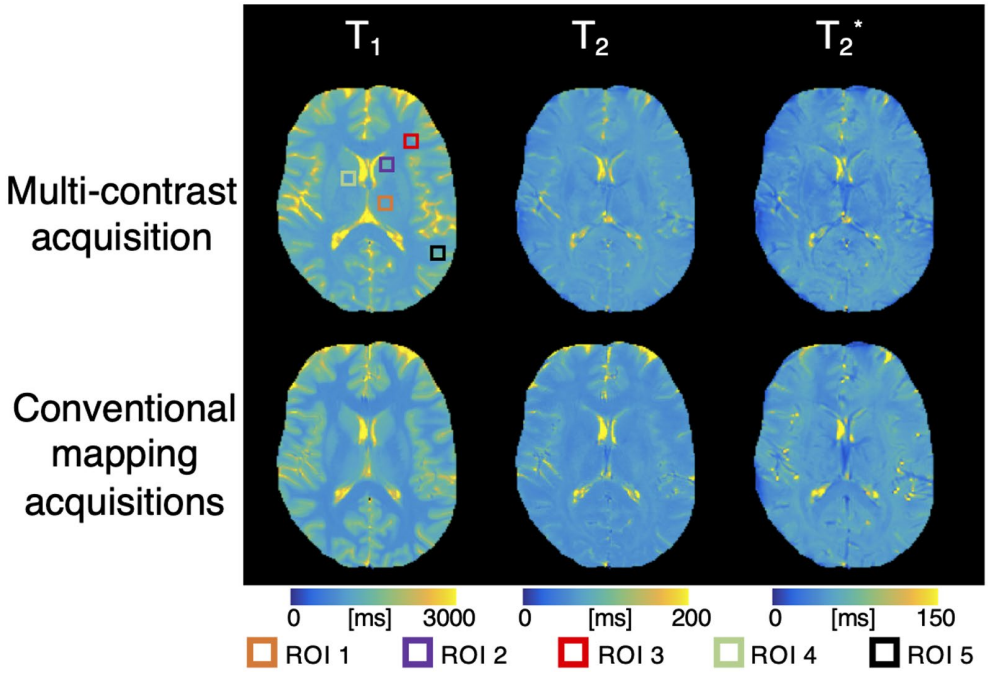

FIGURE 6 Quantitative maps from a multi-shot acquisition of the multi-contrast protocol (top) are compared with quantitative maps derived from conventional mapping approaches (bottom). ROIs from the slice are shown by colored boxes, with values displayed in Figure 7

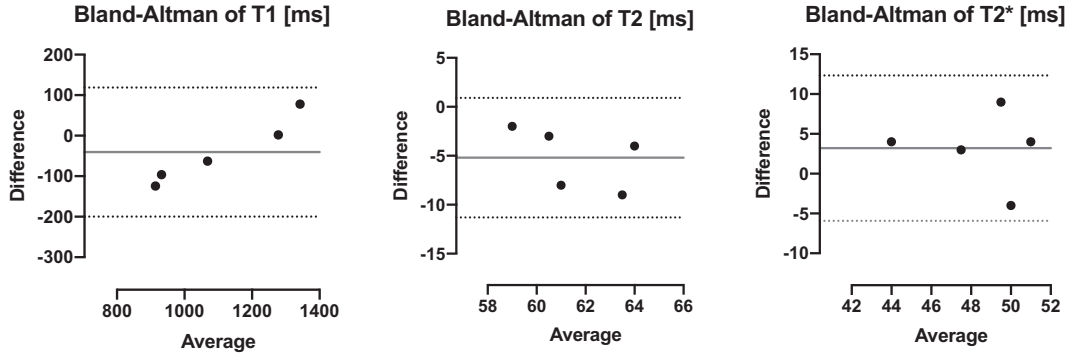

FIGURE 7 Bland-Altman plots showing the mean and difference for the ROIs in Figure 6 for T_1, T_2, and T_2^* values. Although some biases remain, all values are within the limits of agreement

showed slightly higher values in some regions compared to T_2 maps from the conventional multiple spin echo acquisition, possibly due to the differences in acquisition. The T_2 estimated from the multi-contrast EPI approach has only one refocusing pulse and only three asymmetric spin echoes contributing to the T_2 estimation, which may lead to inaccuracies in quantification. Future work to further optimize the TEs, TIs, and total number of time points of this multi-contrast approach may help to improve the accuracy of the maps and further verify the proposed method. Nonetheless, the maps from the different protocols gave reasonably consistent results, and in particular, the SMS acquisition did not strongly affect results. Furthermore, repeated acquisitions of one protocol gave similar results, which is promising for the robustness of the proposed acquisition method.

Additionally, the contrasts in the synthetic images created from the EPI protocols are similar to typical clinical contrasts used in routine MR brain exams, with the exception of the FLAIR image. The FLAIR image does not have the same contrast between gray and white matter due to the smaller MT effects, and additionally, some bright areas can be seen between the gray matter and CSF, likely due to the differences in partial volume effects in the T_1 and T_2 maps. Although the TSE-based scans do not have the typical MT-weighting that is expected, we see overall good agreement between the approaches. Furthermore, through-slice intravoxel dephasing artifacts can be seen in the lower slices using the EPI-based acquisition, which is not present in conventional acquisitions. However, the proposed method has more than three times faster acquisition time for the same resolution and coverage,

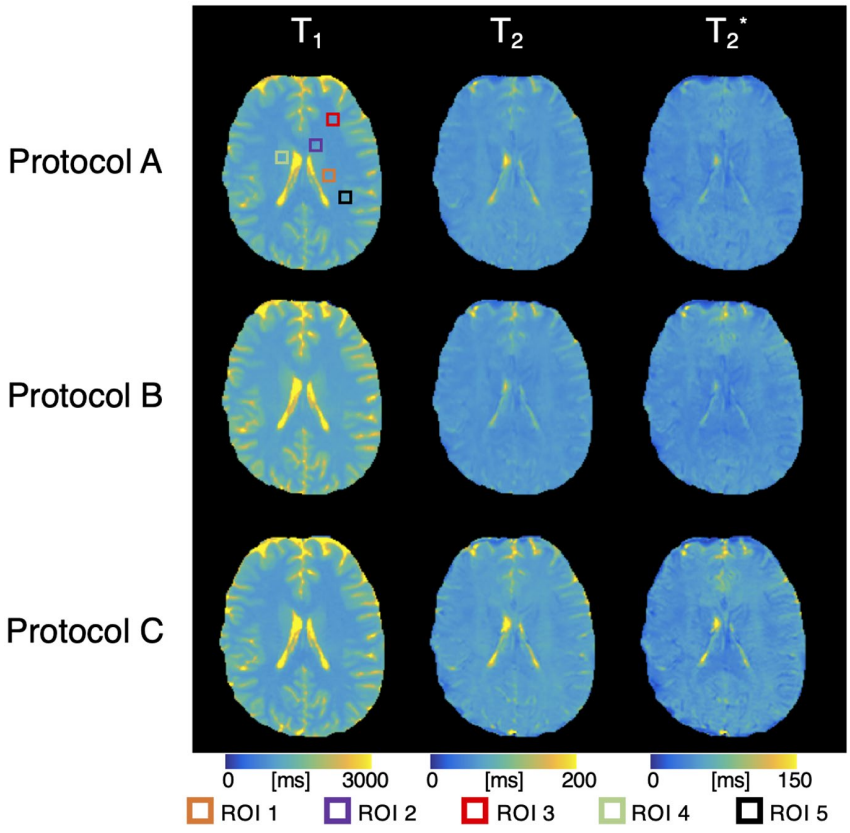

FIGURE 8 Quantitative maps in the same slice from protocols A, B, and C acquired with a global shim in the standard 32-channel coil. ROIs from the slice are shown by colored boxes, with values displayed in Figure 9

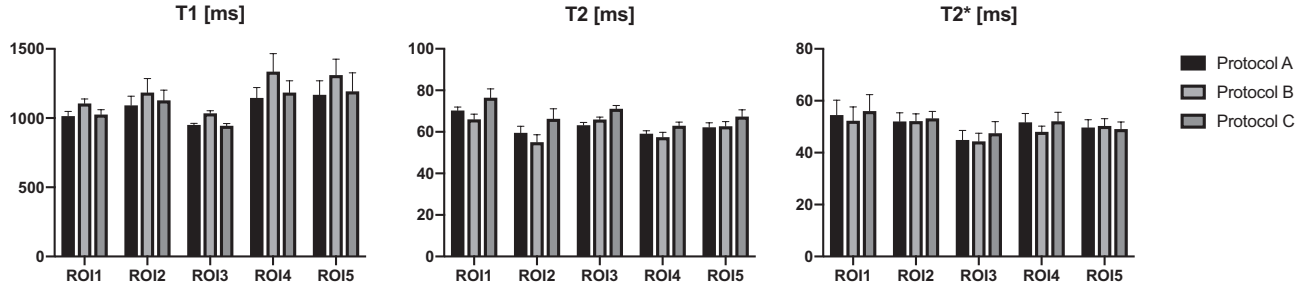

FIGURE 9 Plots showing the mean and SD from the five ROIs shown in Figure 8 for T_1, T_2, and T_2^* values

at the expense of an increase in noise in the synthetic images. In the future, adding MT-weighting may be explored in the proposed approach to better match clinical weightings, and the use of a thinner slice or further improvements in shimming will help alleviate the through-slice intravoxel dephasing artifacts in the lower slices.

The reference scan for parallel imaging contributes to a large percentage of the total scan time. Typically, with EPI acquisitions, the reference scan is also EPI-based so that any distortion is matched between the reference image and the EPI acquisition. However, when we use the presented methods to mitigate distortion, a GRE scan may be sufficient which can reduce coil sensitivity calibration scan time to <5 s. For acquisitions that use dynamic shimming, additional B_0 maps are needed for the slice-optimized MC shimming calibration, which also adds to the overall scan time (~90 s). Recently, a Physics Calibration (PhysiCal)[31] scan consisting of a rapid multi-echo GRE Bloch-Siegert[32-34] acquisition has been proposed to quickly map B0, B1, and RF coil sensitivities for the whole-brain in ~10 s. These fast acquisition maps could not only be used to inform the dynamic shimming calibration, but also eliminate the need for a reference scan for coil sensitivities. Moreover, if needed, the B_0 maps can be used to distort coil sensitivities to match the EPI data to improve parallel imaging reconstruction accuracy. The B_1 mapping provided by the PhysiCal technique would also give additional data to inform the dictionary for estimation of the quantitative maps. In future studies, the PhysiCal approach will be explored to further improve the total scan time as well as the quality of the images and maps.

The multi-shot approach was demonstrated in this work as an alternative to the AC/DC coil for obtaining low distortion EPI images, although it also has the added benefit of a shortened TE for higher resolution. However, the

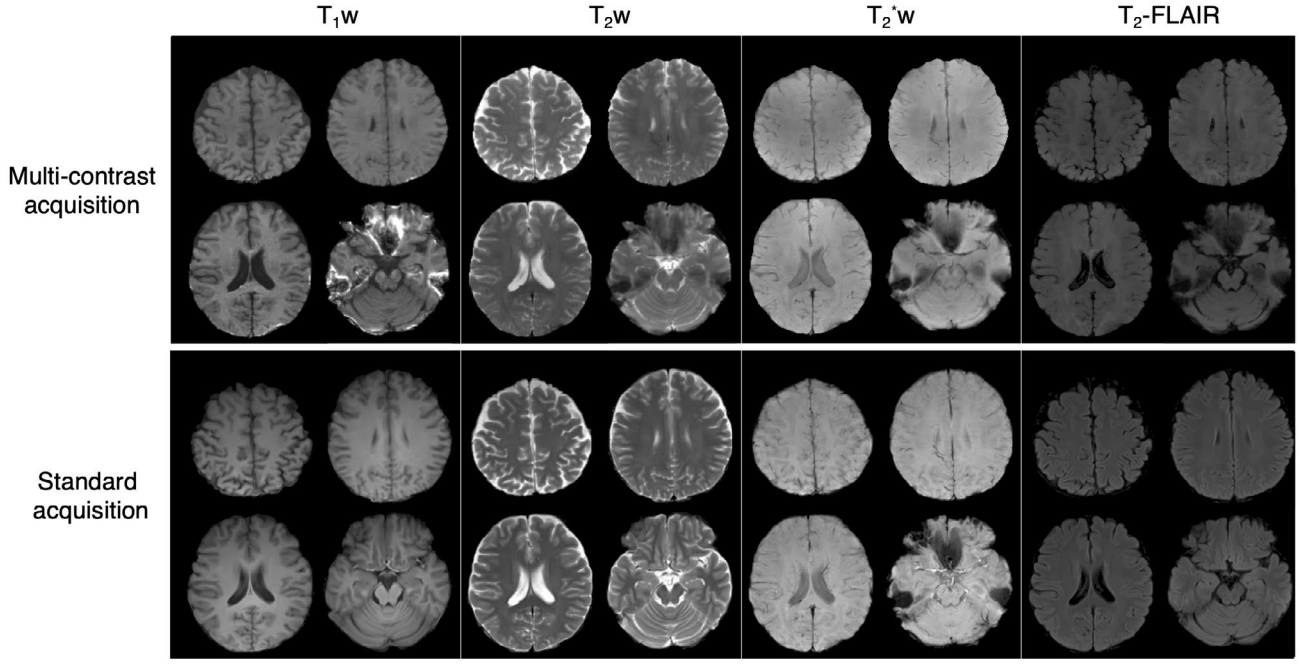

FIGURE 10 Synthetic images created from the proposed protocol (top) are compared to standard brain acquisition methods (bottom) in four slices across the brain. Good agreement is seen between the two methods, although the proposed protocol was acquired 3× faster. The T_2-TSE and T_2-FLAIR images from the proposed method have limited MT weighting compared to the standard acquisitions. Intravoxel dephasing can be seen in the bottom slice in all contrasts in the EPI-based acquisition, as observed in the standard T_2^* image

multi-shot approach comes at the cost of increased scan time. For imaging cases where there are severe B_0 inhomogeneities, it could be beneficial to use both multi-shot and the AC/DC coil together to achieve even larger distortion mitigation.

While multi-shot approaches allow for high acceleration at a relatively high resolution, the resolution and/or acceleration factor may be further improved by implementing low-rank subspace reconstruction techniques.[35-38] This type of reconstruction approach has been demonstrated in several applications where there is temporal information that can be easily modeled in only a few basis functions, such as spectroscopy,[39,40] free breathing dynamic contrast imaging,[41] and quantitative mapping.[35,42,43] These low-rank subspace reconstruction techniques also benefit from complementary and shifted sampling across time, so shifting the k-space sampling across contrasts may be able to be used jointly to improve the reconstruction performance. In future work, shifting k-space sampling across TEs and TIs to increase or better distribute the total number of sampling time points will need to be investigated to optimize the ideal sampling pattern for this type of acquisition. While this type of approach may further improve the resolution and achievable acceleration factor, it also requires an estimate of shot-to-shot phase variation at each T or TI, including differences in phase across shots. Therefore, improved methods to estimate phase, such as directly from the navigator,[44] may be needed to achieve reliable subspace reconstructed images.

In this work, the multi-shot EPI acquisition used a dummy shot to mitigate signal intensity variation across different EPI interleaves. The number of dummy shots could be reduced by reordering the scan so that all repetitions with different TIs of a particular EPI interleave are acquired together in consecutive TRs (for a typical case in our acquisition where the # of TIs > # of EPI-interleaves). However, this reordering increases the amount of time between the data acquisition of the EPI interleaves, allowing for increased shot-to-shot phase corruption and increased potential for motion which must be corrected in reconstruction. Methods to reduce motion artifacts across shots[45-47] using postprocessing techniques may be needed to be implemented in this approach to improve motion robustness.

While the multi-shot reconstruction improves robustness due to respiratory or cardiac motion that causes shot-to-shot phase variation, the presented approach does not account for bulk motion during the scan. In protocols acquired with single-shot EPI, rigid registration between contrasts may help with bulk motion in post-processing. Additionally, motion that occurs between B_0 mapping and the EPI scans will affect the slice-by-slice shimming, although the amount will depend on the degree and direction of the motion. Minimizing the time between B_0 mapping and EPI acquisition should help to mitigate this error, but it remains a limitation of the current method. This effect was investigated by acquiring field maps with different head motions and predicting the shim performance, described in more detail in the Supporting

Information and shown in Supporting Information Figure S4. In summary, while the B_0 maps after motion are somewhat degraded from the optimal shim, there is still an improvement from the original baseline shim by a factor of ~25%, even for dramatic head movements.

The fast approach presented here has several limitations compared to standard brain imaging scans. In its current implementation, the image reconstruction for the multi-shot approach and dictionary matching steps have not been optimized for speed and prohibit the images from being used in real time. The image reconstruction time depends on several factors, including the number of central processing unit (CPU) cores used for parallel imaging, image size, number of shots, number of iterations, and stopping criteria, but should be able to be accelerated by several orders of magnitude using more recently proposed approaches[48,49] for multi-shot reconstruction. Additionally, several approaches for improving dictionary matching speed[50-52] have been proposed using fast group matching, neural networks, and graphics processing units (GPUs) that allow for this step to be completed in less than 1 s per slice. Furthermore, the reduction in scan time comes at the cost of lower resolution and in the cases of the TSE images, slightly different contrast. While the presented method may not be adequate to replace current protocols in cases where subtle lesions or pathology are present, there are several applications where the presented approach may be sufficient and even well-suited due to the fast scan time. For instance, a screening protocol may be beneficial in some emergency situations, such as diagnosing hydrocephalus. The approach also lends itself well to analysis of longitudinal studies during development or aging, where the resolution of the presented protocols may be sufficient. In addition, populations that are prone to motion or cannot tolerate long scans, such as in fetal brain imaging, neonates, and developing high risk children, may benefit from the fast approach presented.

5 | CONCLUSIONS

The approach presented here allows for fast, whole brain imaging with up to 1 mm in-plane resolution to create quantitative parameter maps as well as synthetic images of typical clinical weighted contrasts, generated in 1-4 min. While the images are acquired with EPI, using either dynamic slice-optimized MC shimming or multi-shot reconstruction approaches in combination with in-plane acceleration results in minimal residual distortion, giving the sequence the potential to be used in screening type acquisitions where higher resolution scans may not be needed.

ACKNOWLEDGMENTS

This work was supported in part by NIH research grants: F32EB026304, R01MH116173, R01EB020613, R01EB019437, U01EB025162, P41EB015896, and the shared instrumentation grants S10RR023401, S10RR019307, S10RR019254, S10RR023043.

ORCID

Mary Kate Manhard https://orcid.org/0000-0001-5374-9988
Jason Stockmann https://orcid.org/0000-0001-8454-5347
Congyu Liao https://orcid.org/0000-0003-2270-276X
Sohyun Han https://orcid.org/0000-0002-1309-7628
Merlin Fair https://orcid.org/0000-0002-9100-3105
Berkin Bilgic https://orcid.org/0000-0002-9080-7865

REFERENCES

1. Truong T-K, Darnell D, Song AW. Integrated RF/shim coil array for parallel reception and localized B 0 shimming in the human brain. *Neuroimage*. 2014;103:235-240.
2. Hoffmann J, Shajan G, Scheffler K, Pohmann R. Numerical and experimental evaluation of RF shimming in the human brain at 9.4 T using a dual-row transmit array. *Magn Reson Mater Physics, Biol Med*. 2014;27:373-386.
3. Stockmann JP, Witzel T, Keil B, et al. A 32-channel combined RF and B0 shim array for 3T brain imaging. *Magn Reson Med*. 2016;75:441-451.
4. Chen N, Guidon A, Chang H-C, Song AW. A robust multi-shot scan strategy for high-resolution diffusion weighted MRI enabled by multiplexed sensitivity-encoding (MUSE). *Neuroimage*. 2013;72:41-47.
5. Haldar JP. Low-rank modeling of local k-space neighborhoods (LORAKS) for constrained MRI. *IEEE Trans Med Imaging*. 2014;33:668-681.
6. Mani M, Jacob M, Kelley D, Magnotta V. Multi-shot sensitivity-encoded diffusion data recovery using structured low-rank matrix completion (MUSSELS). *Magn Reson Med*. 2017;78:494-507.
7. Manhard MK, Liao C, Stockmann J, et al. Combined T1, T2, and T2 * mapping using a multi-inversion multi-echo spin and gradient echo EPI sequence. Proc 27th Annu Meet ISMRM, Montr Canada. 2019. Abstract 1189.
8. Warntjes JBM, Dahlqvist O, Lundberg P. Novel method for rapid, simultaneous T1, T2*, and proton density quantification. *Magn Reson Med*. 2007;57:528-537.
9. Krauss W, Gunnarsson M, Andersson T, Thunberg P. Accuracy and reproducibility of a quantitative magnetic resonance imaging method for concurrent measurements of tissue relaxation times and proton density. *Magn Reson Imaging*. 2015;33:584-591.
10. Skare S, Sprenger T, Norbeck O, et al. A 1-minute full brain MR exam using a multicontrast EPI sequence. *Magn Reson Med*. 2018;79:3045-3054.
11. Ordidge RJ, Gibbs P, Chapman B, Stehling MK, Mansfield P. High-speed multislice T1 mapping using inversion-recovery echo-planar imaging. *Magn Reson Med*. 1990;16:238-245.
12. Clare S, Jezzard P. RapidT1 mapping using multislice echo planar imaging. *Magn Reson Med*. 2001;45:630-634.
13. Renvall V, Witzel T, Wald LL, Polimeni JR. Automatic cortical surface reconstruction of high-resolution T1echo planar imaging data. *Neuroimage*. 2016;134:338-354.

14. Schmiedeskamp H, Straka M, Newbould RD, et al. Combined spin- and gradient-echo perfusion-weighted imaging. *Magn Reson Med*. 2012;68:30-40.
15. Eichner C, Jafari-Khouzani K, Cauley S, et al. Slice accelerated gradient-echo spin-echo dynamic susceptibility contrast imaging with blipped CAIPI for increased slice coverage. *Magn Reson Med*. 2014;72:770-778.
16. Larkman DJ, Nunes RG. Parallel magnetic resonance imaging. *Phys Med Biol*. 2007;52:R15-R55.
17. Moeller S, Yacoub E, Olman CA, et al. Multiband multislice GE-EPI at 7 tesla, with 16-fold acceleration using partial parallel imaging with application to high spatial and temporal whole-brain fMRI. *Magn Reson Med*. 2010;63:1144-1153.
18. Feinberg DA, Moeller S, Smith SM, et al. Multiplexed echo planar imaging for sub-second whole brain FMRI and fast diffusion imaging. Valdes-Sosa PA, ed. *PLoS One*. 2010;5:e15710.
19. Setsompop K, Gagoski BA, Polimeni JR, Witzel T, Wedeen VJ, Wald LL. Blipped-controlled aliasing in parallel imaging for simultaneous multislice echo planar imaging with reduced g-factor penalty. *Magn Reson Med*. 2012;67:1210-1224.
20. Liao C, Stockmann J, Tian Q, et al. High-fidelity, high-isotropic-resolution diffusion imaging through gSlider acquisition with and T 1 corrections and integrated Δ B 0 / Rx shim array. *Magn Reson Med*. 2020;83:56-67.
21. Uecker M, Lai P, Murphy MJ, et al. ESPIRiT - An eigenvalue approach to autocalibrating parallel MRI: where SENSE meets GRAPPA. *Magn Reson Med*. 2014;71:990-1001.
22. Uecker M, Lai P, Murphy MJ, et al. ESPIRiT - an eigenvalue approach to autocalibrating parallel MRI: where SENSE meets GRAPPA. *Magn Reson Med*. 2014;71:990-1001.
23. Eichner C, Cauley SF, Cohen-Adad J, et al. Real diffusion-weighted MRI enabling true signal averaging and increased diffusion contrast. *Neuroimage*. 2015;122:373-384.
24. Schmiedeskamp H, Straka M, Bammer R. Compensation of slice profile mismatch in combined spin- and gradient-echo echo-planar imaging pulse sequences. *Magn Reson Med*. 2012;67:378-388.
25. Barral JK, Gudmundson E, Stikov N, Etezadi-Amoli M, Stoica P, Nishimura DG. A robust methodology for in vivo T1 mapping. *Magn Reson Med*. 2010;64:1057-1067.
26. Weigel M, Helms G, Hennig J. Investigation and modeling of magnetization transfer effects in two-dimensional multislice turbo spin echo sequences with low constant or variable flip angles at 3 T. *Magn Reson Med*. 2010;63:230-234.
27. Blystad I, Warntjes JBM, Smedby O, Landtblom AM, Lundberg P, Larsson EM. Synthetic MRI of the brain in a clinical setting. *Acta radiol*. 2012;53:1158-1163.
28. Tanenbaum LN, Tsiouris AJ, Johnson AN, et al. Synthetic MRI for clinical neuroimaging: results of the magnetic resonance image compilation (MAGiC) prospective, multicenter, multireader trial. *Am J Neuroradiol*. 2017;38:1103-1110.
29. Stanisz GJ, Odrobina EE, Pun J, et al. T1, T2 relaxation and magnetization transfer in tissue at 3T. *Magn Reson Med*. 2005;54:507-512.
30. Peters AM, Brookes MJ, Hoogenraad FG, et al. T2* measurements in human brain at 1.5, 3 and 7 T. *Magn Reson Imaging*. 2007;25:748-753.
31. JC, H Z, G D, et al. PhysiCal: A rapid calibration scan for B0, B1+, coil sensitivity and Eddy current mapping. Proc Int Soc Magn Reson Med. Published online. 2020.
32. Sacolick LI, Wiesinger F, Hancu I, Vogel MW. B1 mapping by Bloch-Siegert shift. *Magn Reson Med*. 2010;63:1315-1322.
33. Lesch A, Schlöegl M, Holler M, Bredies K, Stollberger R. Ultrafast 3D Bloch-Siegert B1+-mapping using variational modeling. *Magn Reson Med*. 2019;81:881-892.
34. Corbin N, Acosta-Cabronero J, Malik SJ, Callaghan MF. Robust 3D Bloch-Siegert based B1+ mapping using multi-echo general linear modeling. *Magn Reson Med*. 2019;82:2003-2015.
35. Tamir JI, Uecker M, Chen W, et al. T2 shuffling: Sharp, multicontrast, volumetric fast spin-echo imaging. *Magn Reson Med*. 2017;77:180-195.
36. Dong Z, Wang F, Reese TG, Bilgic B, Setsompop K. Echo Planar Time-Resolved Imaging (EPTI) with subspace constraint and optimized kt trajectory. Proc 27th Annu Meet ISMRM, Montr Canada. 2019, p. 2-4.
37. Liang Z-P. Spatiotemporal imaging with partially separable functions. In: 2007 4th IEEE International Symposium on Biomedical Imaging: From Nano to Macro. IEEE; 2007, p. 988-991.
38. Zhao B, Lu W, Hitchens TK, Lam F, Ho C, Liang Z-P. Accelerated MR parameter mapping with low-rank and sparsity constraints. *Magn Reson Med*. 2015;74:489-498.
39. Lam F, Ma C, Clifford B, Johnson CL, Liang ZP. High-resolution 1H-MRSI of the brain using SPICE: data acquisition and image reconstruction. *Magn Reson Med*. 2016;76:1059-1070.
40. Ma C, Clifford B, Liu Y, Gu Y, Lam F, Yu X, Liang ZP. High-resolution dynamic 31P-MRSI using a low-rank tensor model. *Magn Reson Med*. 2017;78:419-428.
41. Ong F, Lustig M. Beyond low rank + sparse: Multi-scale low rank matrix decomposition. ICASSP, IEEE Int Conf Acoust Speech Signal Process - Proc. 2016;2016-May(4), p. 4663-4667.
42. Christodoulou AG, Shaw JL, Nguyen C, et al. Magnetic resonance multitasking for motion-resolved quantitative cardiovascular imaging. *Nat Biomed Eng*. 2018;2:215-226.
43. Ma S, Nguyen CT, Han F, et al. Three-dimensional simultaneous brain T1, T2, and ADC mapping with MR Multitasking. *Magn Reson Med*. 2020;84:72-88.
44. Wallace TE, Afacan O, Kober T, Warfield SK. Rapid measurement and correction of spatiotemporal B 0 field changes using FID navigators and a multi-channel reference image. *Magn Reson Med*. 2020;83:575-589.
45. Dong Z, Wang F, Ma X, Dai E, Zhang Z, Guo H. Motion-corrected k-space reconstruction for interleaved EPI diffusion imaging. *Magn Reson Med*. 2018;79:1992-2002.
46. Haskell MW, Cauley SF, Wald LL. TArgeted motion estimation and reduction (TAMER): data consistency based motion mitigation for MRI using a reduced model joint optimization. *IEEE Trans Med Imaging*. 2018;37:1253-1265.
47. Cao XC, Liao C, Zhang Z, et al. MOCO-BUDA: motion-corrected blip-up/down acquisition with joint reconstruction for motion-robust and distortion-free diffusion MRI of the brain. In Proceedings of the ISMRM & SMRT Virtual Conference & Exhibition, 2020. Abstract 0465.
48. Aggarwal HK, Mani MP, Jacob M. MoDL-MUSSELS: model-based deep learning for multishot sensitivity-encoded diffusion MRI. *arXiv.* 2018;39:1268-1277.
49. Mani M, Aggarwal HK, Magnotta V, Jacob M. Improved MUSSELS reconstruction for high-resolution multi-shot diffusion weighted imaging. *Magn Reson Med*. 2020;83:2253-2263.
50. Cauley SF, Setsompop K, Ma D, et al. Fast group matching for MR fingerprinting reconstruction. *Magn Reson Med*. 2015;74:523-528.

51. Cohen O, Zhu B, Rosen MS. MR fingerprinting Deep RecOnstruction NEtwork (DRONE). *Magn Reson Med*. 2018;80:885-894.
52. Wang D, Ostenson J, Smith DS. snapMRF: GPU-accelerated magnetic resonance fingerprinting dictionary generation and matching using extended phase graphs. *Magn Reson Imaging*. 2020;66:248-256.

SUPPORTING INFORMATION

Additional Supporting Information may be found online in the Supporting Information section.

FIGURE S1 Two representative slices reconstructed with coil sensitivities found from an EPI calibration scan (top) and a GRE calibration scan (middle). The difference between these two images is shown on the bottom for both slices, at the same windowing, which show consistent reconstructions

FIGURE S2 Quantitative maps from one slice from protocol A, repeated three times. ROIs from the slice are shown by colored boxes, and results from these ROIs are shown in Supporting Information Figure S3

FIGURE S3 Mean values from the five ROIs in Supporting Information Figure S2 for T_1, T_2, and T_2^* maps, where error bars show the standard deviation across the three repeated measurements. No statistically significant differences were found between repeated measures

FIGURE S4 Baseline field maps with different head motions (baseline, nod down, tilt left, and tilt right) are shown on the top, and range from a global std of 29.0-31.3 Hz. The predicted optimized shim from the baseline position was applied to the different head positions to simulate what could be expected if motion occurred between the field map and acquisition (bottom). While resulting field maps are somewhat degraded from the optimal shim (standard deviations range from 20.8-23.0 Hz), there is still an improvement from the original baseline global second order shim by a factor of 25%

How to cite this article: Manhard MK, Stockmann J, Liao C, et al. A multi-inversion multi-echo spin and gradient echo echo planar imaging sequence with low image distortion for rapid quantitative parameter mapping and synthetic image contrasts. *Magn Reson Med*. 2021;86:866–880. https://doi.org/10.1002/mrm.28761